remote sensing

MDPI

Article

Mapping Changes in Fractional Vegetation Cover on the Namib Gravel Plains with Satellite-Retrieved Land Surface Emissivity Data

Laura Obrecht [1,2,*], Frank-Michael Göttsche [1], Johannes Antenor Senn [2] and Jan Cermak [1,3]

[1] Institute of Meteorology and Climate Research, Karlsruhe Institute of Technology, 76021 Karlsruhe, Germany; frank.goettsche@kit.edu (F.-M.G.); jan.cermak@kit.edu (J.C.)
[2] Institute of Geography and Geoecology, Karlsruhe Institute of Technology, 76131 Karlsruhe, Germany; johannes.senn@kit.edu
[3] Institute of Photogrammetry and Remote Sensing, Karlsruhe Institute of Technology, 76131 Karlsruhe, Germany
* Correspondence: laura.obrecht@gmx.de

Abstract: Monitoring changes in vegetation cover over time is crucial for understanding the spatial distribution of rainfall, as well as the dynamics of plants and animals in the Namib desert. Traditional vegetation indices have limitations in capturing changes in vegetation cover within water-limited ecosystems like the Namib gravel plains. Spectral emissivity derived from thermal infrared remote sensing has recently emerged as a promising tool for distinguishing between bare ground and non-green vegetation in arid environments. This study investigates the potential of satellite-derived emissivities for mapping changes in fractional vegetation cover across the Namib gravel plains. Analyzing Moderate Resolution Imaging Spectroradiometer (MODIS) band 29 (λ = 8.55 µm) emissivity time series from 2001 to 2021, our findings demonstrate the ability of both Normalized Difference Vegetation Index (NDVI) and emissivity to detect sudden vegetation growth on the gravel plains. Emissivity additionally allows monitoring the extent of desiccated grass over several years after a rainfall event. Our results support a relationship between the change in fractional vegetation cover, the amount of rainfall and emissivity change magnitude. Information from NDVI and emissivity therefore provide complementary information for assessing vegetation in arid environments.

Keywords: land surface emissivity; thermal remote sensing; MOD21 product; Namib; gravel plains; fractional vegetation cover; NDVI

Citation: Obrecht, L.; Göttsche, F.-M.; Senn, J.A.; Cermak, J. Mapping Changes in Fractional Vegetation Cover on the Namib Gravel Plains with Satellite-Retrieved Land Surface Emissivity Data. *Remote Sens.* **2024**, *16*, 159. https://doi.org/10.3390/rs16010159

Academic Editor: Liming Zhou

Received: 18 November 2023
Revised: 22 December 2023
Accepted: 27 December 2023
Published: 30 December 2023

1. Introduction

Knowledge of fractional vegetation cover (FVC) is important to assess evapotranspiration, photosynthesis and other exchange processes between land surface and atmosphere [1–3]. Remote sensing has become one of the most popular techniques to estimate FVC. The most common methods to estimate FVC from remote sensing data include regression models between FVC and vegetation index (VI) data [4], spectral mixture analysis [5] and linear decomposition of spectral reflectance into vegetation and soil component [6].

However, most vegetation indices commonly used to calculate FVC are not designed for water-limited environments with a vegetative cover of less than 30% and prominence of non-green vegetation [7]. This inability is due to the spectral reflectance of bright desert soils on the one hand and the relatively weak response of the Normalized Difference Vegetation Index (NDVI) to sparse and non-green vegetation on the other hand [8,9].

On the Namib gravel plains, water, in the form of sufficient rainfall, is the most important limiting factor for biomass production. Rainfall is temporally and geographically highly variable [10,11]. It was shown that rainfall decreases and temporal variability of rainfall increases westwards toward the coast [11]. Nevertheless, the grass cover is

an important component in the Namib water and nutrient cycle as well as in complex food webs. Because of the slow turnover rate, often no significant changes in FVC take place over decades [10]. After rare rainfall events, e.g., in 2011, the gravel plains are transformed into highly productive grassland [12,13], as such events decrease the patchiness in the distribution of plants and animals [10]. The short period of rapid growth of grass populations following rainfall events exhausts nutrients faster than they can be replaced and is superseded by a slow rate of decomposition [10]. There is established evidence of the relationship between precipitation and biomass production for the Namib gravel plains [11]. Minimum rainfall requirements for germination and establishment of annual and perennial tussocks range between 10 mm and 25 mm, respectively [14]. The surface response of the Namib gravel plains to rainfall can be explained as the response of plants adapted to water-limited environments [14]. Recent efforts have been taken to map biomass in Namibia on various levels using coarse-resolution NDVI satellite imagery [15]. Mapping changes in FVC on smaller spatial scales holds the potential to monitor the spatial extent and timing of rainfall events [16] and derive biomass information [17] which is important information in a water- and nutrient-limited ecosystem like the Namib, especially since FVC of desert ecosystems is regularly underestimated by up to 44% when calculating FVC from satellite-derived VIs, leading to errors in surface balance and evapotranspiration models [18].

Spectral emissivity information derived from thermal infrared radiance (TIR) can be a valuable instrument to distinguish bare ground from non-green vegetation [19]. At wavelengths from 8 to 9.5 µm, soil minerals like quartz have characteristic low emissivity values due to the 'Reststrahlen' absorption band, while vegetation has a consistently high emissivity throughout the TIR spectrum, independent of plant chlorophyll content. The potential of satellite-retrieved land surface emissivity data has considerably increased with advances in applying the Temperature Emissivity Separation (TES) Algorithm, which was originally developed for the Advanced Spaceborne Thermal Emission and Reflection Radiometer (ASTER), to the Moderate Resolution Imaging Spectroradiometer (MODIS) [19]. Before the arrival of the MOD21 land surface temperature and emissivity (LST&E) product in 2013, applications of satellite-retrieved thermal emissivity data were limited by ASTER's long revisit time (resolution: 90 m, 16 days at best) and the uncertainty of the previous MODIS (MOD11) LST&E product over semi-arid and arid regions, for which land surface emissivities were assigned based on land cover type [20]. Since the TES algorithm works independently from land cover classification, MOD21 emissivities can account for dynamic changes in land surface properties [21]. TES-based emissivities have been applied to monitor rangeland conditions and vegetation phenology on a grassland site at the Jornada Experimental Range in southern New Mexico [9]. Besides a linear trend indicating land cover degradation, the analysis with MODIS band 29 emissivity (e29) time series showed a seasonal cycle, which was attributed to intense rainfall during the monsoon. The rainfall events resulted in increased soil moisture and vegetation cover, which in turn increased emissivity. In contrast, the corresponding MODIS NDVI time series showed near-constant values without any obvious seasonal or linear trends. Ref. [19] demonstrated that the use of a combination of spectral emissivity and NDVI is beneficial to monitor land cover changes associated with agricultural activities. Furthermore, [19] showed the potential of the MOD21 product for monitoring snowmelt over Greenland ice sheets and its value in quantifying land cover change after extreme natural events like fire. The MOD21 product has been available from March 2000 onwards. MODIS band 29 covers the spectral range from 8 to 9.5 µm, which has the largest natural variation in emissivity (from about 0.7 to 0.98). This large variation in spectral emissivity allows observation of changes between proportions of bare soil and non-green vegetation with much greater sensitivity than with VI data [19,22]. In arid environments, temporal changes need to be investigated over long time spans to generate meaningful results. These regions are particularly vulnerable to climate change-induced disturbances that can lead to a high proportional loss of productivity [11].

There is evidence of the relationship between land surface emissivity, NDVI data and FVC [4]. However, the relationship between land surface emissivity and FVC has yet not been explored to detect changes in FVC in an arid ecosystem from satellite-retrieved land surface emissivities. Following [19], a time series analysis of MODIS e29 was conducted over the Namib gravel plains. This is the first study of its kind to not only analyze MOD21 emissivities over more than 20 years, but to also compare its temporal dynamics with independent satellite (NDVI) and field data (rainfall).

In this context, our study focuses on the following objectives:

1. Detection and comparison of changes in emissivity and NDVI time series at multiple sites on the gravel plains and adjacent sand dune sea.
2. Interpretation of observed emissivity changes with the rainfall record of the Gobabeb Namib Research Institute (GNRI), photographs from the gravel plains and corresponding NDVI changes.
3. Finally, we introduce a method to estimate fractional vegetation cover from MOD21 band 29 emissivities and demonstrate its feasibility using existing field measurements.

2. Methods

2.1. Study Site

The Namib is a coastal desert along the Atlantic Ocean. Namib sand dune sea and Namib gravel plains are naturally separated by the ephemeral Kuiseb river (Figure 1). Quartz is the Namib's primary mineral with traces of hematite giving the dunes a dark red color [23]. On the gravel plains, quartz gravel and small pebbles cover the underlying sand [24]. In contrast to the sand dune sea, vegetation on the gravel plains, in form of tufts of grass of a few tens of centimeters, is more prominent because of more frequent but spatially and temporally highly variable rainfall [25]. The dominant grass species and its typical growth patterns are visualized in Figure 2. Further information on vegetation units, diagnostic species and rainfall gradients was summarised by [12,13]. The annual rainfall at Gobabeb varies between 0 and 164 mm with the maximum in 2011 [12].

"Wind" and "Plains" are the Karlsruhe Institute of Technology's (KIT) permanent LST validation stations [26]. This paper will examine and visualize time series of two further test sites on the gravel plains and one test site in the sand dune sea, as previous studies have shown that the gravel plains are structurally homogenous [27]. In the remainder of this paper, the study and test sites will be referred to as given in Table 1. Time series data of other evaluated test sites can be found in the supplementary material (Figure S1). The Namib is an ideal site for validating land surface parameters retrieved from satellite remote sensing data as it has a high frequency of clear sky conditions and is spatially and temporally stable due to its arid climate [26].

Table 1. Geographic location of the study and test site pixels evaluated during the emissivity and NDVI time series analysis. Available data for the FVC change validation.

Site Name	Geographic Location	Available Data
Study site 1 (Wind)	−23.55°S, 15.05°E	Rain record, field photographs, NDVI and emissivity time series
Study site 2 (Plains)	−23.52°S, 15.08°E	Field photographs, NDVI and emissivity time series
Test site 1	−23.54°S, 15.17°E	NDVI and emissivity time series
Test site 2	−23.45°S, 15.39°E	NDVI and emissivity time series
Test site 3 (Dunes)	−23.55°S, 14.93°E	NDVI and emissivity time series

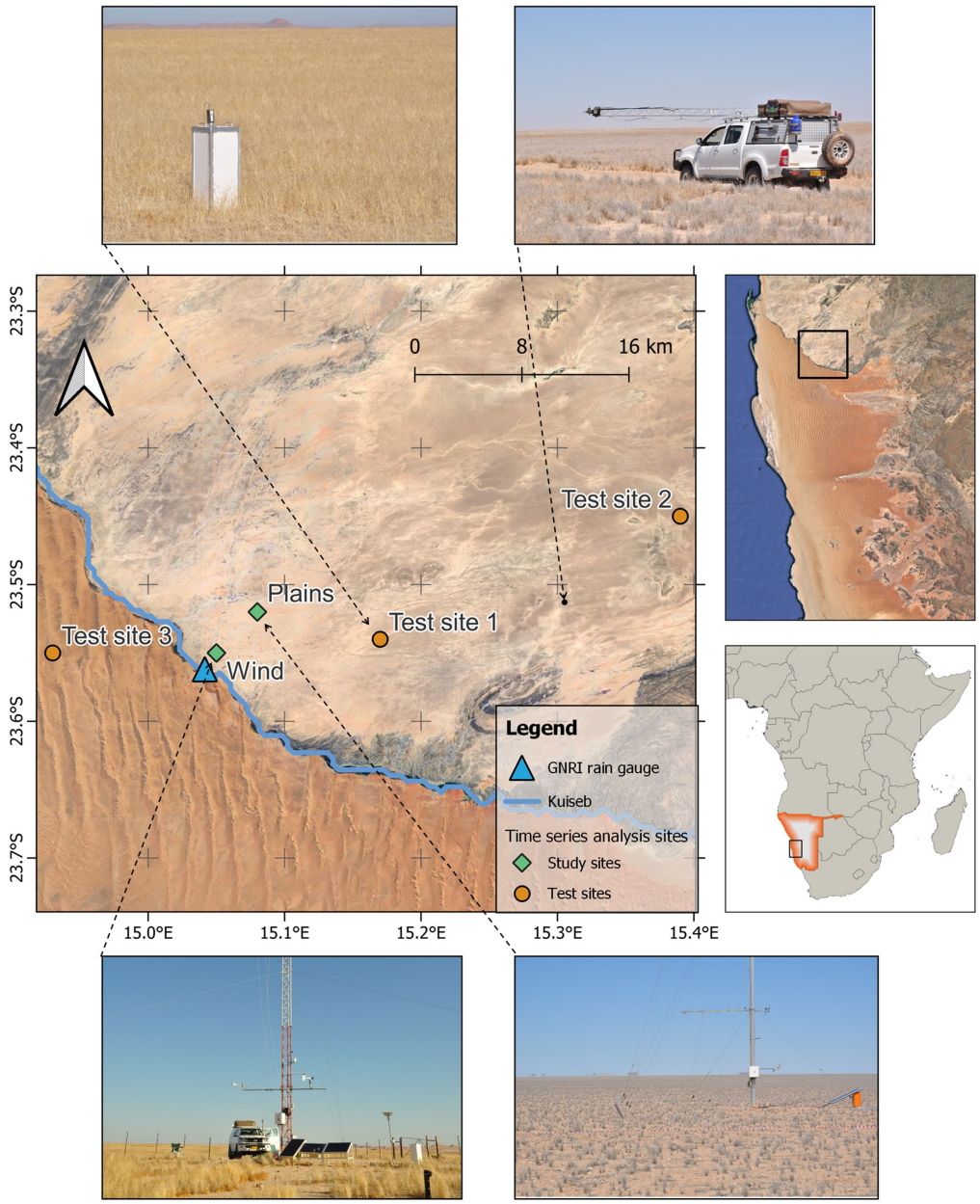

Figure 1. Locations used for MOD21 emissivity time series analysis. Background: Google Earth. The Namib sand dune sea and the gravel plains are sharply separated by the Kuiseb river (blue).

Figure 2. Left: Dominant grass species on the gravel plains: *Stipagrostis ciliata*. The gravel plains are covered with grass after an unusually heavy rain event in early 2011. Picture taken in November 2011 near Wind. **Right**: Picture taken in February 2013 at Plains.

2.2. Change Detection with BFAST

Breaks for Additive Season and Trend (BFAST) is a change detection algorithm, which has been applied to a range of time series with varying noise levels and can deal with seasonal and non-seasonal time series from multiple disciplines [28,29]. We applied BFAST to the 21-year MODIS emissivity and NDVI time series using the BFAST package for the R statistical software (version 4.2.2) [30] to separate significant changes from residual noise in the time series.

The BFAST method uses an additive model that decomposes time series data (Yt) on pixel-scale into trend (Tt), seasonal (St) and residual (et) components (1):

$$Yt = St + Tt + et \quad (1)$$

Changes occurring in the trend component are a strong indicator of disturbances, whereas the seasonal component reflects phenological changes [29]. Breakpoints are returned and linear trend compartments between breakpoints are fitted via linear regression. The change magnitude is the difference between the time series value before and after a breakpoint [29]. We ran BFAST for each site (Table 1) with the monthly mean emissivity and NDVI time series from 2001 to 2021 as input. We did not use a seasonal model, motivated by the highly infrequent rain events in the Namib, which do not allow for phenological changes [12]. Change magnitudes are regarded as significant if they are greater than the emissivity standard deviation at the test site Dunes during the monitoring period ($sd_{\varepsilon,Dunes}$ = 0.006). Ref. [31] showed that BFAST is especially successful in arid environments where trend breaks are indicators of biomass changes and closely follow rainfall patterns.

The year 2011 was the wettest on record for the gravel plains [12] and is therefore of particular interest for this study to assess spatial patterns in the land cover response of emissivity and NDVI to rainfall. We visualized the change magnitude of MODIS emissivity and NDVI in 2011 over the Namib gravel plains and sand dune sea near Gobabeb using the BFASTspatial package. The BFASTspatial package provides utilities to perform change detection analysis on time series of remote sensing images [32]. We used the monthly mean emissivity raster composites of all cloud-free acquisitions of the study site from January 2010 to December 2012 as input.

2.3. Datasets and Data Preparation

The applied workflow is visualized in Figure 3. The datasets used are discussed in more detail in the following subsections.

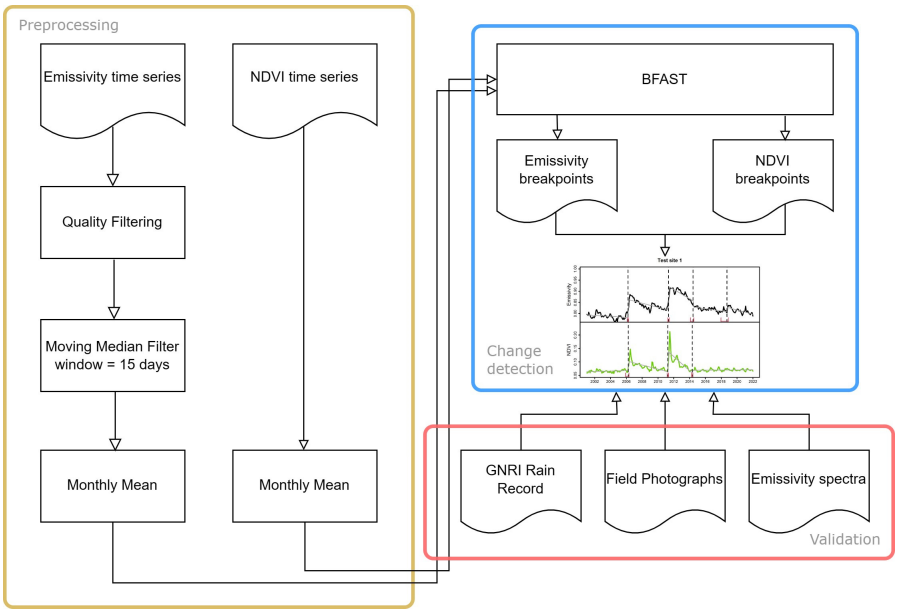

Figure 3. Analysis workflow performed in this study.

2.3.1. Satellite-Based Data

MODIS onboard of Terra covers 36 discrete spectral bands from 0.4 µm to 14.4 µm with a spatial resolution of 250 m to 1 km. We obtained MOD21 (LST&E) and MOD13 (NDVI) datasets covering the study area from January 2001 to December 2021 from the NASA Earthdata Search [33] and downloaded the datasets with AppEEARS. A summary of both MODIS datasets is presented in Table 2. In total, we obtained 7526 MOD21 and 488 MOD13 scenes. The results presented here use a subset of the tile h19v11, covering parts of the gravel plains and the sand dune sea.

Table 2. Summary of MODIS datasets used in this study.

Data Product	Spatial Resolution	Temporal Resolution
Terra MODIS LST&E (MOD21)	L3 Global 1 km	1 day
Terra MODIS Vegetation Indices (MOD13)	L3 Global 500 m	16 days

Emissivity: MOD21 Product.

The spectral emissivity $\varepsilon(\lambda)$ is a dimensionless quantity, defined as the ratio of a material's thermal radiance at wavelength λ to the radiance emitted by an ideal black body at the same temperature. MOD21 is a daily level-3 LST&E product with a nominal spatial resolution of 1 km at nadir. In this study, only daytime observations from MODIS are used. MODIS band 29 covers the spectral range from 8 to 9.5 µm and contains the largest natural variation in emissivity (from about 0.7 to 0.98). Analyzing MOD21 time series, low band 29 emissivities (<0.85) indicate a high fraction of bare soil exposure, whereas higher values (up to 0.96) indicate a high FVC in the respective MODIS pixel [19]. Band 32 (11 µm) can theoretically be used to distinguish between dry and green vegetation [19]. However, over the Namib gravel plains, the dynamic range of emissivity in band 29 is about four times larger than that in band 32. Therefore, band 29 was analyzed rather than band 32, although narrow band emissivity derived in band 32 is less affected by atmosphere. Furthermore, for the hyper-arid Namib desert, retrieval errors due to uncertainty in atmospheric water vapor are generally less significant [34]. Recent studies investigating the accuracy of the MOD21 product have shown that it has an accuracy of 1% in the Namib desert [34].

We used three quality criteria from the quality control MOD21 scientific dataset to exclude clouds and noise from the retrieved MOD21 scenes. Around 3500 good-quality observations remained for further processing for each site (see supplementary material for details, Table S1). We applied a moving median filter with a window length of 15 days to the MOD21 band 29 emissivity time series to reduce TES retrieval noise and to match the temporal resolution of 16 days of the NDVI product. In the next step, we resampled the time series to monthly mean values to remove outliers, e.g., due to undetected clouds. The resulting time series of monthly MODIS band 29 emissivities from 2001 to 2021 consisted of 252 data points.

Normalized Difference Vegetation Index (NDVI): MOD13 NDVI.

The NDVI is defined as in Equation (2):

$$NDVI = \frac{NIR - R}{NIR + R} \quad (2)$$

where *NIR* is the land surface reflectance in the near-infrared and *R* the reflectance corresponding to the red band [35]. In this study, we employ the NDVI, since its relationship with FVC is well understood, long consistent time series are available and because of its widespread use in remote sensing applications. The NDVI is, furthermore, an easily calculated dimension, without the need for site-specific coefficients, like, for example, the Soil-Adjusted Vegetation Index (SAVI) [36,37].

The MOD13 product provides an NDVI dataset at a spatial resolution of 500 m and a temporal resolution of 16 days. The NDVI data are obtained from daily surface reflectance.

With a MODIS-specific compositing method, only good-quality NDVI values are kept and the highest value closest to nadir is selected to represent the compositing period [7]. The NDVI time series was smooth with no significant noise; therefore, no further quality filtering was performed. We resampled the NDVI values to monthly mean NDVI, which from 2001 to 2021 resulted in a time series of monthly NDVI values of 252 data points.

Time series of both products were created by extracting emissivity and NDVI values from the pixels closest to the locations presented in Table 1. The larger range of viewing geometries represented by the MOD13 product (a 16-day composite) means that its field of view (FOV) is randomly located within the larger pixel area of the respective MOD21 product (1 day). Based on this and the gravel plains' high spatial homogeneity, both products were directly compared despite their different pixel sizes.

2.3.2. Field Photographs

Photographs taken on site can provide qualitative information on the vegetation state at a given time and location. Since 2007, members of the KIT satellite climatology research group take photographs regularly during field trips to the Namib, where KIT operates two permanent LST validation sites [27]. The photographs are not standardized but allow us to qualitatively reconstruct the vegetation development on the gravel plains. Therefore, each picture available from the KIT validation sites "Wind" and "Plains" from 2007 to September 2022 was assigned to an FVC class from one for "bare ground", to four for "green grass cover" (see Table 3). The resulting time series consisted of 18 and 12 data points for Wind and Plains, respectively.

Table 3. Vegetation states on the Namib gravel plains, based on photographs.

FVC Class	Vegetation State
1	Bare ground
2	Patchy, light-grey, dry grass
3	Patchy, yellow dry grass
4	Green grass cover

2.3.3. Rainfall Record

We incorporated monthly rainfall data into the analysis to validate changes detected in the NDVI and emissivity time series as rainfall-associated vegetation growth. We make use of the observational rainfall data recorded by the GNRI at their meteorological station. The dataset consists of the monthly sums of precipitation recorded from 1962 to 2021 at GNRI. Because of the proximity of the meteorological station to the KIT LST validation site "Wind" (Figure 1), we use the record to validate rainfall-associated vegetation growth at the study site Wind. The same record was analyzed in depth in [12]. With the dominance of plants that are adapted to water limitation, the land surface responds to rainfall with immediate grass growth [11].

2.3.4. Lab- and In-Situ-Retrieved Emissivity Spectra

Thermal infrared emissivity spectra link the satellite-retrieved emissivity to the spectral characteristics of the study area. Emissivity spectra are regularly used to validate satellite-retrieved emissivity [23,38]. Emissivity spectra for samples of land surface types relevant to the Namib gravel plains (namely dry grass, gravel and sand) were obtained in the laboratory by NASA's Jet Propulsion Laboratory (JPL) using a Frontier Perkin-Elmer-Spectrometer. Furthermore, during a field campaign in 2017, in-situ emissivity spectra were obtained with a BOMEM MR304SC FTIR spectroradiometer. Further details on the field protocols are provided by [27]. We calculated MODIS band 29 channel effective emissivities for the three samples as well as for the in-situ spectra by convolving the emissivity spectra with the MODIS spectral response function from the "Satellite Sensor Relative Spectral Response data" [39] (Table 4, Figure 4). As explained in Section 2.3.1, only band 29 is used for the time series analysis, as emissivity variation in this spectral range is the largest (Figure 4).

Over the hyper-arid Namib gravel plains, retrieval errors due to uncertainty in atmospheric water vapor are generally less significant [34].

Table 4. MODIS band 29 channel effective emissivities and standard deviations within band 29 of relevant surface types on the Namib gravel plains obtained from laboratory emissivity spectra and for in-situ emissivity spectra for KIT stations Wind and Plains.

	Sample	MODIS Band 29 Channel Effective Emissivity	Standard Deviation
Lab Spectra	Grass	0.961	0.001
	Gravel	0.799	0.020
	Sand	0.783	0.020
In-situ Spectra	Wind	0.830	0.009
	Plains	0.810	0.015

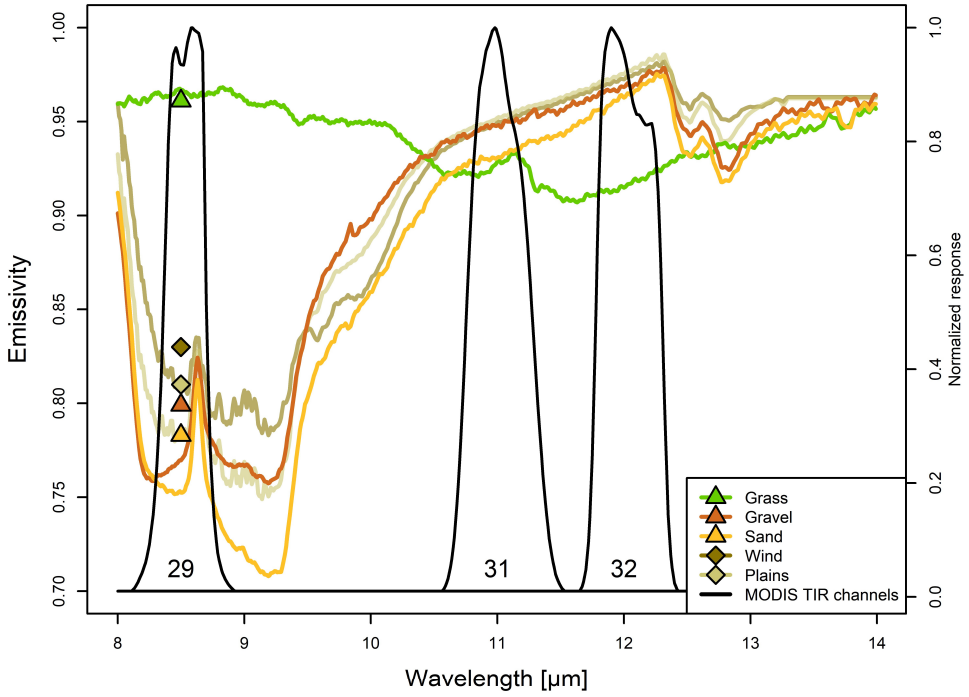

Figure 4. Thermal infrared (8–14 µm) emissivity spectra of dry grass, gravel and sand samples determined in the laboratory (data courtesy: G. Hulley, JPL, USA) and in-situ (data courtesy: L. Poutier, ONERA, France) at study sites Wind and Plains. Triangles and squares represent the laboratory and in-situ samples' channel effective emissivities, respectively. Shown in black are the normalized response functions of MODIS bands 29, 31 and 32.

These channel effective emissivities are used in Section 3.3 to demonstrate how a relationship between in-situ and satellite data can be used to estimate FVC from MOD21 band 29 emissivity. The method assumes that the gravel plains' land surface behaves like a Lambertian reflector and that MOD21 band 29 emissivity can be regarded as the linear combination of the emissivities of gravel and dry grass ($\varepsilon_{29,gravel}$ and $\varepsilon_{29,grass}$). On the Namib gravel plains, in the absence of other vegetation types, FVC is assumed to represent the fraction of grass, see Equation (3), which is adapted from [40,41].

$$\varepsilon_{29} = \varepsilon_{29,\,grass} * FVC + \varepsilon_{29,\,gravel} * (1 - FVC) \quad (3)$$

To account for indirect radiance reaching the sensor due to internal reflections, introduced Equation (4), which scales the contribution of a cavity term $d\varepsilon$ via a quadratic relationship with FVC. $d\varepsilon$ is the additional emissivity due to the indirect radiance reaching

the sensor via reflections between floor and walls of the roughness element (here the sides of the grass [42]). Over grasslands, this contribution is zero when the surface is either bare (FVC = 0.0) or fully covered by grass (FVC = 1.0), i.e., when internal scattering is negligible.

$$\varepsilon = \varepsilon_{29,grass} * FVC + \varepsilon_{29,gravel} * (1 - FVC) + 4 * d\varepsilon * FVC(1 - FVC) \quad (4)$$

To derive the site-specific cavity term $d\varepsilon$, we used image-classification-based FVC values of the about 10 m^2 FOV of the two radiometers mounted at 25 m at the Wind mast from April 2011, which have an overall classification accuracy of more than 97% [24]. By inserting the FVC values determined by [24] and the corresponding mean MOD21 band 29 emissivity for April 2011 ($\varepsilon_{29,\text{April 2011}}$) as well as the channel effective emissivities for gravel and dry grass ($\varepsilon_{29,\text{gravel}}$ and $\varepsilon_{29,\text{grass}}$), an estimation of $d\varepsilon$ is obtained, which characterizes the grass population on the gravel plains (Table 5). Solving Equation (4) by [42] for the FVC, FVC is a function of the root of ε_{29} (5):

$$FVC\ (\varepsilon_{29}) = \frac{\varepsilon_{29,grass} - \varepsilon_{29,gravel} + 4d\varepsilon - \sqrt{\left(\varepsilon_{29,grass} - \varepsilon_{29,gravel} + 4d\varepsilon\right)^2 + 16d\varepsilon\left(\varepsilon_{29,gravel} - \varepsilon_{29}\right)}}{8d\varepsilon} \quad (5)$$

Table 5. FVC derived from image classification of the two radiometers' FOV [24] and their corresponding $d\varepsilon$ derived from Equation (4).

Radiometer	FVC	$d\varepsilon$
Radiometer 1	17%	0.059
Radiometer 2	26%	0.025
Mean	21.5%	0.039

3. Results

This section presents the results obtained from the NDVI and emissivity time series analysis with BFAST. While we evaluated time series at multiple locations, we put a special emphasis on the location Wind, as this location is closest to the GNRI rain gauge and the vegetation development is best documented by field photographs.

3.1. Change Detection with BFAST

Variations in emissivity at test site 3 (Dunes) were small. Band 29 emissivities were stable over time with only one significant breakpoint in 2011. The other breakpoints detected by the BFAST algorithm are negligible due to their small change magnitudes, which were smaller than the standard deviation of emissivity before 2011 at Dunes ($sd_{\text{emissivity,Dunes}}$ = 0.006, Table 6). Between 2001 and 2011, the average emissivity was 0.781, which is in good agreement with the MODIS band 29 channel effective emissivity for the sand lab spectrum ($\varepsilon_{29,\text{sand}}$ = 0.783, Table 4). After the breakpoint in 2011, the average emissivity has increased to 0.797, which is 2% higher than the sand channel effective emissivity.

For the NDVI time series at test site 3, a breakpoint in 2011 was detected by the BFAST algorithm as well, but its change magnitude is lower than the corresponding NDVI standard deviation (Table 6).

Analyzing emissivity and NDVI time series provides insights into the surface dynamics on the gravel plains over the 21-year observation period: emissivity and NDVI values over the gravel plains are subject to considerable change throughout this period (Figures 5 and 6). We detected a minimum of three breakpoints at each site and four at test site 1 and study site 1. Change magnitudes differed considerably among the sites. The seasonal component calculated with BFAST was for all sites on the gravel plains below the standard deviation at Dunes. BFAST was therefore run with no seasonal model.

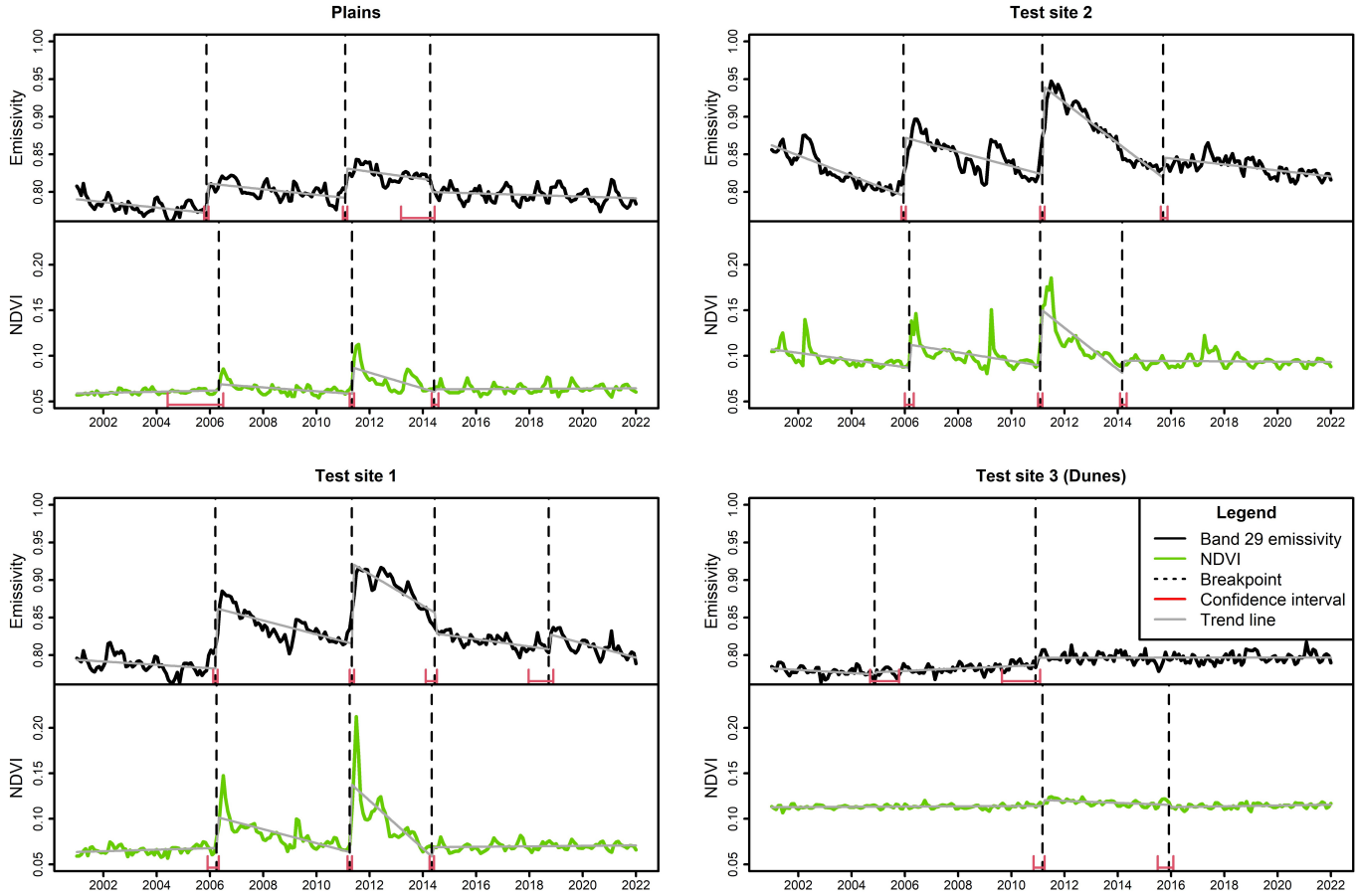

Figure 5. Emissivity (top panel, black) and NDVI (bottom panel, green) time series for the sites on the gravel plains and sand dune sea (test site 3). Trend line segments and breakpoints with confidence intervals (red) determined by BFAST.

Table 6. Change magnitude of emissivity and NDVI determined for the two study sites (Wind and Plains) and the three test sites (1 and 2 on the gravel plains, 3 in the sand dune sea) for each breakpoint determined by BFAST. Breakpoint 3 can be neglected, see Figure 5.

Breakpoint	Plains		Wind		Test Site 1		Test Site 2		Test Site 3 (Dunes)	
	Emissivity	NDVI	Emissivity	NDVI	Emissivity	NDVI	Emissivity	NDVI	Emissivity	NDVI
I	0.039	0.007	0.032	0.014	0.08	0.033	0.077	0.025	0.003	-
II	0.039	0.028	0.059	0.054	0.105	0.074	0.116	0.06	0.013	0.006
III	−0.016	0.003	−0.01	0.011	−0.028	0.01	0.026	0.013	-	-
IV	-	-	0.028	0.015	0.019	-		-	0.006	−0.003

Comparing the emissivity breakpoints between the sites on the gravel plains gives a uniform picture of their timing (Table 7). The breakpoints in 2005/2006 and 2011 were detected at all sites on the gravel plains (i.e., test site 3 in the sand dune sea is ignored) and lie within a period of four months. A break in 2018 (breakpoint IV) was only detected for some locations with a higher temporal difference and uncertainty of timing (Figure 5). NDVI values show similar temporal changes but smaller change magnitudes (Table 6). Breakpoints in the NDVI time series match the emissivity breakpoints closely with a maximum time difference of 4 months (Table 7). After a breakpoint, NDVI values decrease over three months to about one-third of the corresponding peak value and then slowly decrease further to their 'pre-breakpoint' levels (NDVI = 0.05 to 0.10). In contrast, emissivity increases quickly to a maximum value and then decreases nearly linearly over a period of three to five years to its 'pre-breakpoint' level, with typical values of ε_{29} = 0.80 to 0.85

(Figure 6). The channel effective emissivity obtained from the in-situ emissivity spectrum at Wind ($\varepsilon_{29,Wind}$ = 0.83, Table 4) fits the MOD21 band 29 emissivity values in years of steady emissivity at the study site Wind (i.e., when the BFAST trend line has a slope of nearly zero).

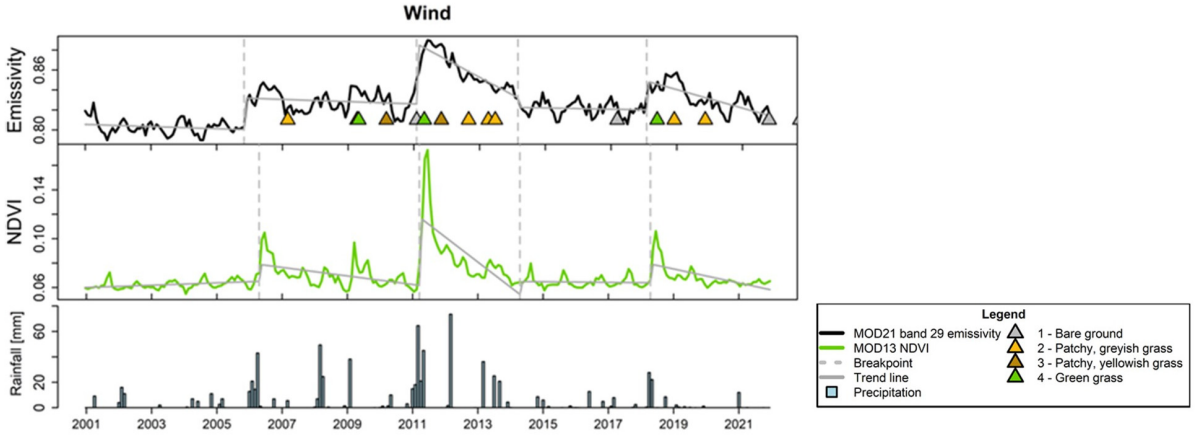

Figure 6. Emissivity (top panel), NDVI (middle panel) and rainfall (bottom panel) time series at the study site Wind from 2001 to 2021. Triangles indicate dates with documented vegetation state by field photographs taken at the KIT Wind mast.

Table 7. Emissivity breakpoints detected by BFAST at study and test sites. Time difference Δ to NDVI breakpoints is in months. Positive values indicate an NDVI breakpoint detected after the corresponding emissivity breakpoint, negative values an NDVI breakpoint before the emissivity breakpoint. Non-significant breakpoints (i.e., change magnitude < 0.006) are shown in parentheses.

	Breakpoint I		**Breakpoint II**		**Breakpoint III**		**Breakpoint IV**	
Site	Month	Δ	Month	Δ	Month	Δ	Month	Δ
Wind	2005-12	4	2011-03	0	(2014-04)	0	2018-03	1
Plains	2005-12	4	2011-02	2	(2014-04)	1	-	-
Test site 1	2006-04	−1	2011-05	−2	(2014-06)	−2	2018-09	-
Test site 2	2006-01	1	2011-03	−2	2015-09	−19	-	-
Test site 3 (Dunes)	(2004-12)	-	2010-12	4	-	-	(2017-11)	

3.1.1. Breakpoint Analysis with GNRI Rainfall Record

The three breakpoints associated with an increase in emissivity and NDVI at the location Wind (breakpoint I, II and IV) coincide with almost 40% (~300 mm) of the rainfall during the 21-year monitoring period. Around breakpoint II, more than 20% of the total rainfall precipitated. The three breakpoints have in common that it rained for at least two consecutive months to break emissivity and NDVI values. During these two months, between 53 and 166 mm of rainfall precipitated (Figure 7). The rain events in 2008 and 2012 did not cause a break in the NDVI or emissivity time series, although 80 (73) mm rain precipitated over a period of 3 (1) months, respectively (Figure 6). While the time series for the study site Wind and test sites 1 and 2 show increases in emissivity and NDVI in early 2009, these changes are not detected by the BFAST algorithm.

Emissivity increases, especially for heavier rainfall events like in 2011, over several months. In contrast, NDVI starts to increase later and rises more steeply. Change magnitudes are highest around the rainfall event in 2011 and considerably smaller in 2005/2006 and 2018, when only 92.3 mm and 53.2 mm precipitated, respectively (Figure 7). Assuming a simple linear model for precipitation and change magnitude yielded an R^2 of 0.96. With respect to the entire rainfall record, the period from 2006 to 2012 was a considerably wetter period with several small rainfall events each year. We suggest that the wetter regime increased the emissivity background level, i.e., the emissivity trend line is approximately

horizontal, but has a higher intercept (Figure 6). The corresponding NDVI values peak in 2006 and 2009, parallel to the rainfall events.

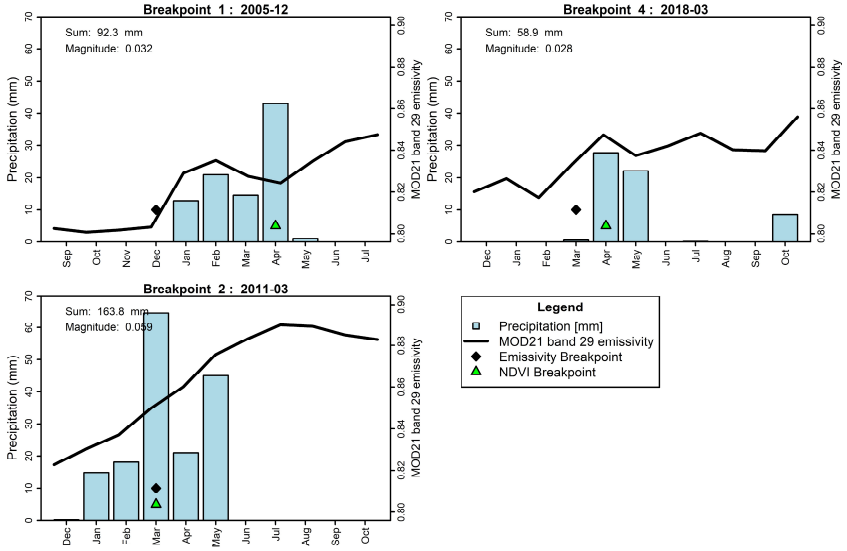

Figure 7. Rain (mm) around the breakpoints at Wind in 2005, 2011 and 2018. The course of the MOD21 band 29 emissivity is drawn on to the bar plot. Sum of rainfall and change magnitude is given in the top left corner of the plots.

3.1.2. Breakpoint Analysis with Field Photographs

The gravel plains are rarely bare during the observation period (see supplementary material for more photographs, Figures S2 and S3), which fits the MOD21 band 29 emissivity at the study sites being constantly higher than the gravel channel effective emissivity ($\varepsilon_{29,gravel}$ = 0.799).

After the rain events in early 2011, NDVI and emissivity at the location Wind increased up to 0.17 and 0.88, respectively. The germination of grass populations is documented by photographs from April 2011 (Figure 8). By November 2011, NDVI has already decreased to <0.10. In contrast, the emissivity is still close to its level from March, i.e., $\varepsilon_{29,Nov/2011}$ = 0.87. Field photographs show that many parts of the gravel plains are covered by dry grass in November 2011 (Figure 8). By the end of 2012, the grass has turned grey, and the distribution has become patchier (Figure 8), but emissivity values of $\varepsilon_{29,Dec/2012}$ = 0.85 suggest that the patchy grass cover still influences the emissivity, while NDVI values have returned to their initial values of 0.06 from 2010. Similar values are obtained for July 2013: dry grass populations covering the gravel plains in patches are still visible (Figure 8) and the emissivity retrieved for Wind is $\varepsilon_{29,Jul/2013}$ = 0.843, while NDVI dropped to around 0.06. After the last rain event in 2018, grass cover has constantly decreased, which fits the decreasing emissivity trend line after 2018 in Figure 6. In September 2022, the gravel plains were practically bare (personal communication F. Göttsche).

3.2. Change Detection with BFASTspatial

With the raster-stack based implementation of BFAST in R, we were able to identify spatially coherent zones of significantly increased MODIS band 29 emissivities and to set the findings of the previous section into a spatial context. Evaluating change magnitudes across the entire MODIS emissivity subset reveals hotspots in the central and north-eastern parts with strongly increasing emissivities in 2011 (Figure 9). In the sand dune sea, change magnitudes are close to zero and confirm the findings of the time series analysis at test site 3 (Dunes). Generally, change magnitudes increase toward the eastern part of the study area. We also recognized this pattern during the BFAST change detection for the emissivity.

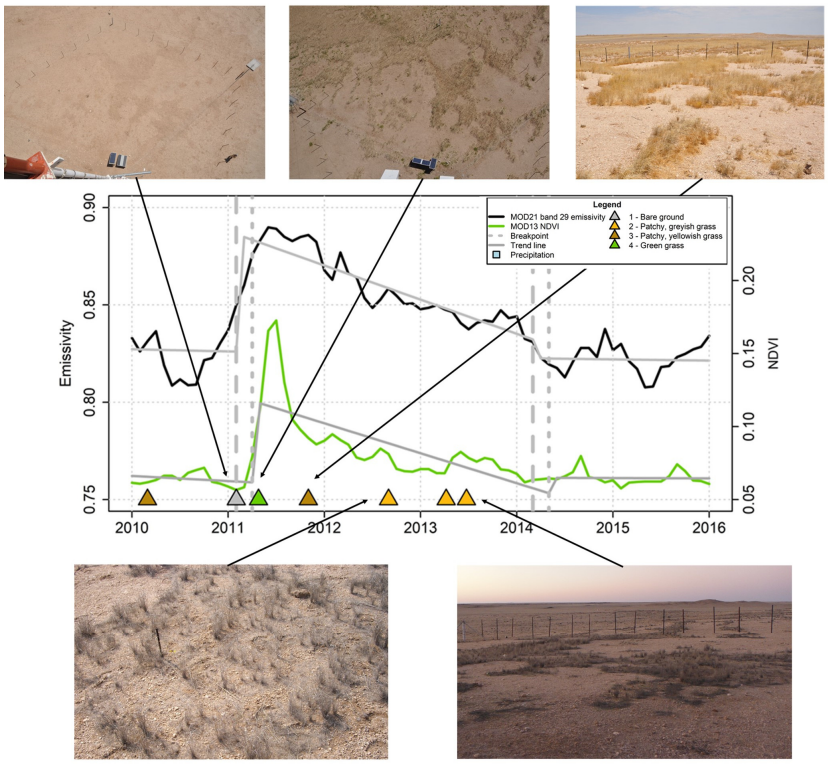

Figure 8. NDVI and emissivity subset from 2010 to 2016. Field photographs corresponding to color-coded triangles.

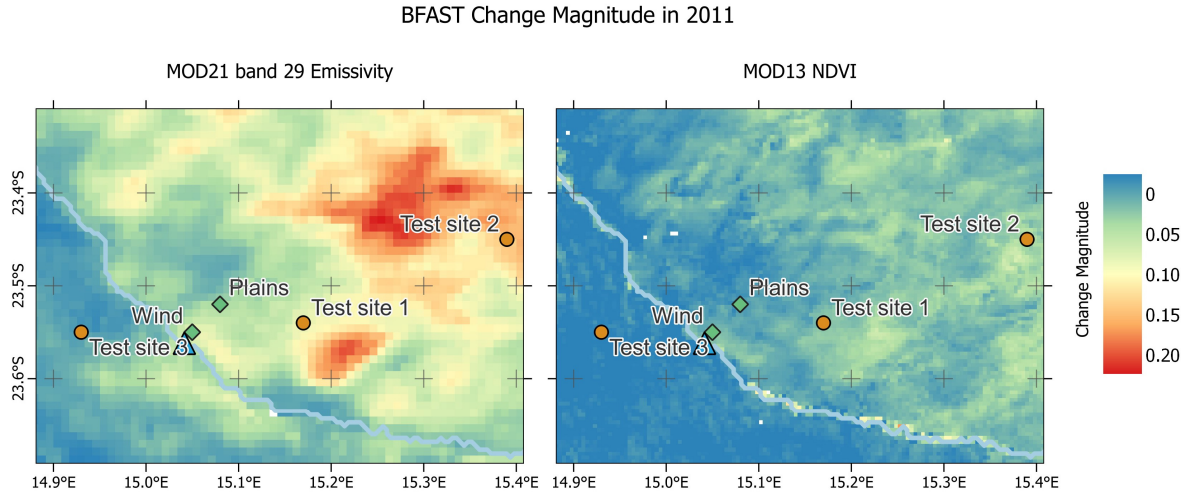

Figure 9. Visualization of change magnitude of the emissivity and NDVI time series in 2011. The course of the ephemeral Kuiseb River is depicted in transparent blue. X-and y-axes show longitude and latitude, respectively.

The greatest NDVI change magnitude is observed around the ephemeral Kuiseb river and almost no change in the sand dune sea. On the gravel plains, NDVI increased only marginally, with a maximum magnitude of 0.06. The smaller change magnitudes determined for the NDVI time series may also be a relic from the BFAST algorithm: by fitting a linear trend line to the decrease after a breakpoint, the NDVI peak values are higher than the trend line suggests. Maximum NDVI values are up to 0.25 for some locations (Figure 6). We believe a non-linear function (e.g., an exponential decay function) would better describe the NDVI decrease. While the peak emissivity values are also

underestimated, the trend lines fit the emissivity time series considerably better (Wind: R^2 = 0.85 and 0.64 for emissivity and NDVI, respectively) (Figure 6).

3.3. Potential for Estimating FVC

Based on the promising results for detecting changes in FVC, we want to explicitly encourage further research in quantifying FVC from MOD21 band 29 emissivity. Therefore, this paragraph showcases a potential method for estimating FVC from MOD21 band 29 emissivity. While the obtained results are consistent and plausible, stringent validation needs to be the topic of future research, mainly due to insufficient ground truth data.

Figure 10 shows the FVC estimated with Equations (3) and (4), i.e., with the linear mixture model ("Linear") and with the three different cavity terms from Table 5, respectively. The non-linear model with the cavity term outperforms the linear mixture model, as it accounts for internal scattering processes, which are prominent in partly vegetated areas, and thereby avoids FVC overestimation. Since the FVCs determined for the two radiometers via image classification from field photographs reflect the natural variation in the grass cover in the proximity of the Wind mast, the two curves "Radiometer 1" and "Radiometer 2" in Figure 10 indicate the uncertainty interval in calculated FVC due to uncertainty in the cavity term. The uncertainty increases with increasing FVC and decreases again when FVC approaches 1.0. While the presented approach needs further research, it provides a first estimate that is realistic according to local site knowledge [24,27], with the most frequent FVC being less than or equal to 0.1 and the highest FVC of 0.25 during 2011 at the study site Wind (results for using the mean cavity term). The development of the grass cover can be visualized by calculating the FVC across monthly mean MOD21 band 29 composites using the mean $d\varepsilon$ value from Table 5 (Figure 11). The resulting distribution and gradient of FVC during 2011 from southwest to northeast fits the local rainfall gradient reported in [12]. To assess the accuracy of the simplified cavity term by [42] and to validate the proposed method, form parameters of grass populations [41] and in-situ FVC values must be obtained at multiple locations on the gravel plains—ideally, over the 1 km^2 MODIS pixel size—and the cavity term calculated manually.

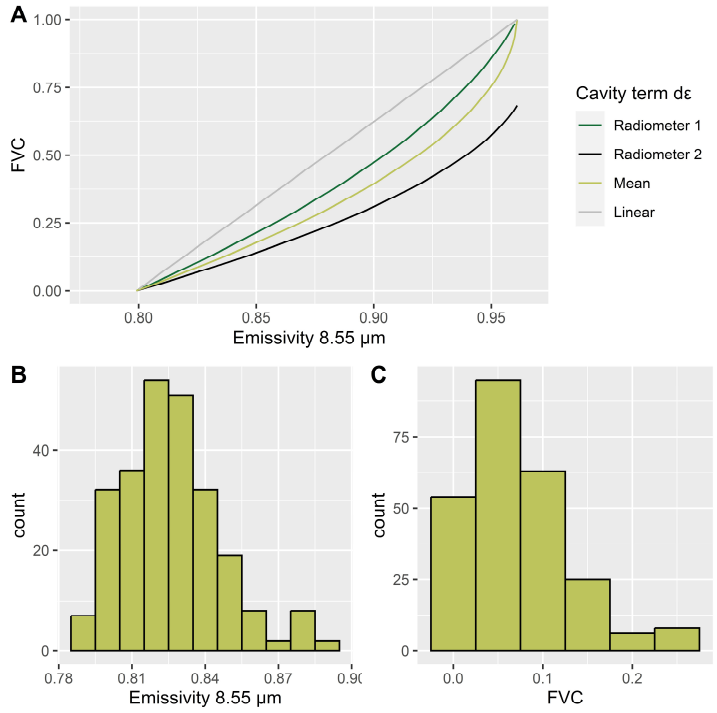

Figure 10. (**A**) FVC as a function of emissivity considering different values for the cavity term (Radiometer 1 and 2, their mean) as well as the linear mixture model (Linear), (**B**) Frequency distribution of MOD21 band 29 emissivity (8.55 µm) and (**C**) Frequency distribution of derived FVC with mean cavity term. The monthly emissivity time series from 2001 to 2021 at study site Wind is used.

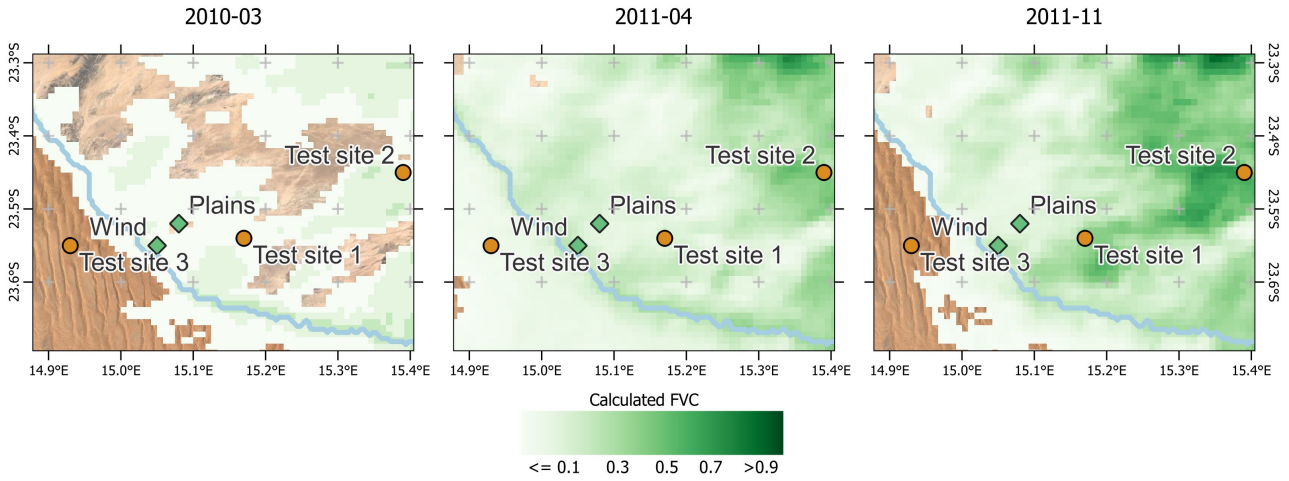

Figure 11. FVC calculated with Equation (5) and mean $d\varepsilon$ for the monthly mean emissivity composites corresponding to the first three photographs in Figure 6. Background: Google Earth image, visible for calculated FVC less than or equal to zero.

4. Discussion

Analyses of MODIS thermal emissivity data over the period from 2001 to 2021 on the Namib gravel plains show periods and regions of strongly increasing, and afterward steadily decreasing, band 29 land surface emissivities. Rising emissivity values coincide with rain events and peaks in the corresponding NDVI time series, and can be linked to an increase in grass cover on the Namib gravel plains. In the following, we will discuss the results in the context of vegetation cover change. Effects on LSE other than FVC change are evaluated and the applicability of the presented findings discussed.

4.1. Results in Context of FVC Change

The lab and in-situ emissivity spectra of the Namib land surface samples fit the MOD21 band 29 retrieved emissivity over the sand dune sea and gravel plains. This supports the ability to map land cover features of the study area based on its satellite-retrieved spectral characteristics reported by [23,38]. The low temporal variability of emissivity over the 21-year time series at test site 3 (Dunes) agrees with [21], who found low temporal variations in MOD21 band 29 emissivity time series for a similar site in terms of mineralogy and climatology: the Algodones Dunes, California, USA. A possible explanation for the 2% higher emissivity values after 2011 at test site Dunes in the sand dune sea can be vegetation growth in interdune sections [23], which seems to be supported by a small increase in NDVI (Figure 5). Wind-blown vegetation detritus is often trapped in these sections [10]. The observed emissivity dynamics on the gravel plains are in good agreement with results from other studies. Band 29 emissivity is a function of FVC: low band 29 emissivities (<0.85) indicate a high fraction of bare soil exposure, whereas higher values (up to 0.961) indicate a high FVC in the respective MODIS pixel [9,19].

Considering the NDVI time series, the present findings are in good agreement with [43] who report increasing NDVI values of up to 0.13 after precipitation events during the growing season in the hyper-arid Heihe River Basin, China. However, such low NDVI values must be interpreted carefully. Ref. [44] retrieved the reflectance of various substrates in the laboratory using a LICOR spectrometer and calculated an NDVI of 0.202 for quartzite, which is not significantly different from the peak NDVI values at the evaluated sites on the gravel plains. Previous research has classified pixels with NDVI < 0.2 as bare soil, i.e., the gravel plains would be classified as permanent bare soil [45], leading to errors in surface energy balance and evapotranspiration models [18]. Emissivity and NDVI are useful for detecting sudden vegetation growth. However, the NDVI's rapid decline and inherent ambiguity make it unsuitable for mapping vegetation cover in arid environments. Emissivity additionally provides the capability to monitor dry biomass, i.e., the amount of

desiccated grass on the Namib gravel plains, as it remains elevated for several years, i.e., it also reflects grass populations that turned dry and grey. Ref. [9] confirmed that inter-annual changes in vegetation regardless of seasonality are better observed in emissivity data than in VI data.

In the context of field campaigns on the gravel plains, increases in emissivity and NDVI can be interpreted as the signal of growing annual grass species combined with resprouting of perennial species [10,14,46]. The surface response of the Namib gravel plains to rainfall events is biomass production [11]: rainfall events trigger grass growth, which increases the FVC and, because of the different material and multi-scattering effects of plant matter, increases emissivity [19]. This explains why rainfall amount and emissivity change magnitude are linked, which was shown for the analyzed breakpoints at the study site Wind. When considering the increasing rain regime toward the northeast and the resulting higher emissivity change magnitudes and higher FVC, the learned link also fits the other sites. Spatial and temporal variations in FVC extend over several years and are triggered by considerable and rare rain events [11]. The time series analysis indicates a spatial gradient of FVC with increasing values toward the northeast, which agrees with the findings by [11] and with the known rainfall gradient on the Namib gravel plains [10–12].

Our results suggest that breaks associated with multiple rain events spread out over several months are detected with greater certainty by the BFAST algorithm than isolated rain events. Especially for 2011, the 95% confidence interval of the breakpoint is only three months. This was also noted by [47]. Ref. [10] found that, due to the nutrient limitation of the Namib, a rainfall event of considerable magnitude only two years after an earlier event did not cause a comparable response, although the total rainfall was similar (~100 mm). This finding is a possible explanation for why isolated rain events following the rain event in early 2011 do not show up in the emissivity time series. Two events caused increased emissivity values, but BFAST did not detect corresponding breaks in the time series. This issue could be accounted for by increasing the number of possible breakpoints (h-value) [47].

4.2. Effects on LSE Other Than FVC Change

The TES algorithm is central to the reliable retrieval of MOD21 emissivities. Generally, the algorithm works best over semi-arid and arid regions with a considerable fraction of bare soils and low water content in the atmosphere [48]. This is also where TES emissivities are most needed since over dense vegetation emissivity is generally well known and does not vary much [48]. In the following section, possible effects on the emissivity–FVC relationship will be discussed.

4.2.1. Directional View Angle Effects

MODIS sensors view the locations of interest from east or west. The viewing zenith angles reach values up to 60°. An overestimation of the FVC for viewing angles greater than 40° must be considered because the radiation emitted by a partially vegetated area is higher than that emitted by an individual roughness element [4,41]. The anisotropy of MOD21 emissivities over arid regions was investigated by [49]. We tested for directional view angle effects by limiting view angle observations to less than 15°. The emissivity values in the resulting time series did not decrease, nor did the filtering affect the BFAST breakpoints and their respective change magnitudes. Directional view angle effects can, therefore, be neglected for the time series analysis, but should be considered for the FVC calculation; however, temporal resampling and applying a moving median filter considerably decreased directional view angle effects for the FVC estimation.

4.2.2. Soils and Soil Moisture

Emissivity, particularly in the 8 to 9 µm range, increases with increasing soil moisture due to water adhering to soil grains and decreasing the reflectance in that region. This effect is especially relevant in arid regions with sandy soils and low water contents [50].

Though with a high sensible heat flux and a potential evaporation rate of 3000 mm per year in the Namib [51], soil moisture cannot be the cause of elevated emissivity values over a period of multiple months to years. The usefulness of emissivity data is reduced over soils with a high clay content and low quartz content, since this increases the emissivity in the 8 to 9 µm spectral range. Fortunately, the Namib gravel plains consist of minerals with a high amount of quartz and little clay and field measurements have shown that emissivity is highly stable [27].

4.3. Limitations

FVC validation data have been frequently obtained by field sampling [8,52], object-based image analysis or aerial photographs [18,53]. For our study, in-situ estimates of FVC were scarce and only available at the two study sites (Wind, Plains). Therefore, we limited the study to detecting FVC change and assigning FVC classes. This was feasible thanks to the Namib's slow vegetation dynamics and field photographs taken at intervals of a few months to a year. We were able to assign all greening events visible in field photographs at Wind and Plains to elevated emissivity values; conversely, elevated emissivity values could be related to FVC changes visible in the field photographs. Nevertheless, by introducing a method to also obtain quantitative data on FVC from emissivity for the Namib gravel plains in paragraph 3.3, we want to give a perspective on what will be feasible with additional in-situ FVC data from field campaigns and photographs.

5. Conclusions and Outlook

In a water- and nutrient-limited ecosystem such as the Namib, knowledge of biomass distribution is important information. By analyzing time series of emissivity, NDVI and rainfall we demonstrated how the responses of emissivity and NDVI to rainfall events on the Namib gravel plains differ. Strong increases in MOD21 band 29 emissivity matched peaks in NDVI time series and considerable rainfall events of more than 50 mm. After such rainfall events, NDVI responds to the germination and greening of grass populations with sharp peaks and, therefore, can be used to detect sudden vegetation growth. Emissivity additionally provides the capability to monitor dry biomass, e.g., the amount of desiccated grass. The approach was applied to MODIS emissivity time series and yielded promising results for mapping FVC changes on the Namib gravel plains. FVC change was also estimated from field photographs and corresponded to changes in MOD21 band 29 emissivity. Spatial patterns of change magnitude fit the regional rainfall gradient and suggest a relationship between FVC, rainfall amount and emissivity change magnitude. In this context, our study is the first of its kind as it presents an integrated analysis of FVC change by analyzing rainfall data, field photographs, NDVI and emissivity time series. BFAST proved to be a robust change detection instrument and a good choice for identifying change in time series with negligible seasonality. However, the method could be extended to include non-linear functions, e.g., to model NDVI decrease in arid environments.

The results presented in this study are promising for FVC estimation in arid environments since emissivity does not depend on chlorophyll content, i.e., it is sensitive to desiccated as well as green vegetation. This is door-opening for a new methodology to calculate FVC from emissivity, which we outlined in Section 3.3. Furthermore, developing a relationship between MODIS emissivity and FVC holds, in our opinion, great potential for its simplicity and availability of MODIS emissivity data. Validation of the estimated FVC and its spatial patterns requires additional in-situ data, which will also allow investigation of the link between emissivity and FVC in more detail. In-situ FVC data and information on species distribution will be of great value to understanding the unique responses of annual and perennial species to rain events on the gravel plains. Finally, time series of data from thermal sensors with higher spatial resolutions, e.g., ECOSTRESS onboard the International Space Station, would allow extending the approach to regions that are less homogeneous than the Namib gravel plains.

Supplementary Materials: The following supporting information can be downloaded at: https://www.mdpi.com/article/10.3390/rs16010159/s1, Table S1. Number of masked observations per site and filter; Figure S1. Emissivity and NDVI time series of additional sites on the gravel plains; Figure S2. Selection of field photographs at LST validation site Wind from 2007 until 2022; Figure S3. Selection of field photographs at LST validation site Plains from 2011 until 2022.

Author Contributions: Conceptualization, F.-M.G. and L.O.; Methodology, L.O.; Formal Analysis, L.O.; Resources, F.-M.G.; Writing—Original Draft Preparation, L.O.; Writing—Review and Editing, F.-M.G., L.O., and J.A.S.; Visualization, L.O.; Supervision, J.C. and J.A.S.; Project Administration, J.C. All authors have read and agreed to the published version of the manuscript.

Funding: This research received no external funding.

Data Availability Statement: The MODIS datasets used in this work are publicly available online through NASA Earthdata: "https://www.earthdata.nasa.gov/ (accessed on 5 March 2023)".

Acknowledgments: We would like to thank the Gobabeb Namib Research Institute and Roland Vogt from the University of Basel, Switzerland for providing us with the rainfall data. We kindly thank Elsa Abbott and Glynn Hulley from NASA JPL for the Namib lab spectra and Laurent Poutier from ONERA for the in-situ spectra from the LST validation sites Wind and Plains. Finally, we would like to thank the KIT Satellite Climatology research group for the field photographs and their research on the Namib gravel plains, which provided the foundation on which this paper is built.

Conflicts of Interest: The authors declare no conflict of interest.

References

1. Prince, S.D. Satellite Remote Sensing of Primary Production: Comparison of Results for Sahelian Grasslands 1981–1988. *Int. J. Remote Sens.* **1991**, *12*, 1301–1311. [CrossRef]
2. Schimel, D.S.; House, J.I.; Hibbard, K.A.; Bousquet, P.; Ciais, P.; Peylin, P.; Braswell, B.H.; Apps, M.J.; Baker, D.; Bondeau, A.; et al. Recent Patterns and Mechanisms of Carbon Exchange by Terrestrial Ecosystems. *Nature* **2001**, *414*, 169–172. [CrossRef] [PubMed]
3. Nemani, R.R.; Running, S.W.; Pielke, R.A.; Chase, T.N. Global Vegetation Cover Changes from Coarse Resolution Satellite Data. *J. Geophys. Res. Atmos.* **1996**, *101*, 7157–7162. [CrossRef]
4. Wittich, K.-P. Some Simple Relationships between Land-Surface Emissivity, Greenness and the Plant Cover Fraction for Use in Satellite Remote Sensing. *Int. J. Biometeorol.* **1997**, *41*, 58–64. [CrossRef]
5. Song, W.; Mu, X.; Ruan, G.; Gao, Z.; Li, L.; Yan, G. Estimating Fractional Vegetation Cover and the Vegetation Index of Bare Soil and Highly Dense Vegetation with a Physically Based Method. *Int. J. Appl. Earth Obs. Geoinf.* **2017**, *58*, 168–176. [CrossRef]
6. Zhang, X.; Liao, C.; Li, J.; Sun, Q. Fractional Vegetation Cover Estimation in Arid and Semi-Arid Environments Using: HJ-1 Satellite Hyperspectral Data. *Int. J. Appl. Earth Obs. Geoinf.* **2013**, *21*, 506–512. [CrossRef]
7. Huete, A.; Didan, K.; Miura, T.; Rodriguez, E.P.; Gao, X.; Ferreira, L.G. Overview of the Radiometric and Biophysical Performance of the MODIS Vegetation Indices. *Remote Sens. Environ.* **2002**, *83*, 195–213. [CrossRef]
8. Jiapaer, G.; Chen, X.; Bao, A. A Comparison of Methods for Estimating Fractional Vegetation Cover in Arid Regions. *Agric. For. Meteorol.* **2011**, *151*, 1698–1710. [CrossRef]
9. French, A.N.; Schmugge, T.J.; Ritchie, J.C.; Hsu, A.; Jacob, F.; Ogawa, K. Detecting Land Cover Change at the Jornada Experimental Range, New Mexico with ASTER Emissivities. *Remote Sens. Environ.* **2008**, *112*, 1730–1748. [CrossRef]
10. Seely, M.K.; Louw, G.N. First Approximation of the Effects of Rainfall on the Ecology and Energetics of a Namib Desert Dune Ecosystem. *J. Arid. Environ.* **1980**, *3*, 25–54. [CrossRef]
11. Henschel, J.R.; Burke, A.; Seely, M. Temporal and Spatial Variability of Grass Productivity in the Central Namib Desert. *Afr. Study Monogr.* **2005**, *30*, 43–56.
12. Eckardt, F.D.; Soderberg, K.; Coop, L.J.; Muller, A.A.; Vickery, K.J.; Grandin, R.D.; Jack, C.; Kapalanga, T.S.; Henschel, J. The Nature of Moisture at Gobabeb, in the Central Namib Desert. *J. Arid. Environ.* **2013**, *93*, 7–19. [CrossRef]
13. Juergens, N.; Oldeland, J.; Hachfeld, B.; Erb, E.; Schultz, C. Ecology and Spatial Patterns of Large-Scale Vegetation Units within the Central Namib Desert. *J. Arid. Environ.* **2013**, *93*, 59–79. [CrossRef]
14. Seely, M.K. The Namib Dune Desert: An Unusual Ecosystem. *J. Arid. Environ.* **1978**, *1*, 117–128. [CrossRef]
15. Westinga, E.; Beltran, A.P.R.; de Bie, C.A.J.M.; van Gils, H.A.M.J. A Novel Approach to Optimize Hierarchical Vegetation Mapping from Hyper-Temporal NDVI Imagery, Demonstrated at National Level for Namibia. *Int. J. Appl. Earth Obs. Geoinf.* **2020**, *91*, 102152. [CrossRef]
16. Du Plessis, W.P. Linear Regression Relationships between NDVI, Vegetation and Rainfall in Etosha National Park, Namibia. *J. Arid. Environ.* **1999**, *42*, 235–260. [CrossRef]
17. Eisfelder, C.; Kuenzer, C.; Dech, S. Derivation of Biomass Information for Semi-Arid Areas Using Remote-Sensing Data. *Int. J. Remote Sens.* **2012**, *33*, 2937–2984. [CrossRef]

18. Geng, X.; Wang, X.; Fang, H.; Ye, J.; Han, L.; Gong, Y.; Cai, D. Vegetation Coverage of Desert Ecosystems in the Qinghai-Tibet Plateau Is Underestimated. *Ecol. Indic.* **2022**, *137*, 108780. [CrossRef]
19. Hulley, G.; Veraverbeke, S.; Hook, S. Thermal-Based Techniques for Land Cover Change Detection Using a New Dynamic MODIS Multispectral Emissivity Product (MOD21). *Remote Sens. Environ.* **2014**, *140*, 755–765. [CrossRef]
20. Wan, Z.; Dozier, J. A generalized split-window algorithm for retrieving land-surface temperature from space. *IEEE Trans. Geosci. Remote Sens* **1996**, *34*, 892–905.
21. Hulley, G.C.; Malakar, N.K.; Islam, T.; Freepartner, R.J. NASA's MODIS and VIIRS Land Surface Temperature and Emissivity Products: A Long-Term and Consistent Earth System Data Record. *IEEE J. Sel. Top. Appl. Earth Obs. Remote Sens.* **2018**, *11*, 522–535. [CrossRef]
22. French, A.N.; Schmugge, T.J.; Kustas, W.P. Discrimination of Senescent Vegetation Using Thermal Emissivity Contrast. *Remote Sens. Environ.* **2000**, *74*, 249–254. [CrossRef]
23. Hulley, G.; Hook, S. Intercomparison of Versions 4, 4.1 and 5 of the MODIS Land Surface Temperature and Emissivity Products and Validation with Laboratory Measurements of Sand Samples from the Namib Desert, Namibia. *Remote Sens. Environ.* **2009**, *113*, 1313–1318. [CrossRef]
24. Bork-Unkelbach, A. Extrapolation von in-situ Landoberflächentemperaturen auf Satellitenpixel. Ph.D. Thesis, Karlsruher Institut für Technologie, Karlsruhe, Germany, 2012.
25. White, F. The Vegetation of Africa. *Nat. Resour. Res.* **1983**, *20*, 356.
26. Göttsche, F.; Hulley, G. Validation of Six Satellite-Retrieved Land Surface Emissivity Products over Two Land Cover Types in a Hyper-Arid Region. *Remote Sens. Environ.* **2012**, *124*, 149–158. [CrossRef]
27. Göttsche, F.; Olesen, F.; Poutier, L.; Langlois, S.; Wimmer, W.; Santos, V.G.; Coll, C.; Niclos, R.; Arbelo, M.; Monchau, J.-P. Report from the Field Inter-Comparison Experiment (FICE) for Land Surface Temperature. *Identity* **2017**, *9*, 0929b3d2a06f1e6010.
28. Morrison, J.; Higginbottom, T.P.; Symeonakis, E.; Jones, M.J.; Omengo, F.; Walker, S.L.; Cain, B. Detecting Vegetation Change in Response to Confining Elephants in Forests Using MODIS Time-Series and BFAST. *Remote Sens.* **2018**, *10*, 1075. [CrossRef]
29. Verbesselt, J.; Hyndman, R.; Newnham, G.; Culvenor, D. Detecting Trend and Seasonal Changes in Satellite Image Time Series. *Remote Sens. Environ.* **2010**, *114*, 106–115. [CrossRef]
30. Verbesselt, J.; Masiliunas, D.; Zeileis, A.; Appel, M. Bfast: Breaks for Additive Season and Trend. Available online: https://bfast2.github.io/ (accessed on 1 December 2022).
31. Browning, D.M.; Maynard, J.J.; Karl, J.W.; Peters, D.C. Breaks in MODIS Time Series Portend Vegetation Change: Verification Using Long-Term Data in an Arid Grassland Ecosystem: Verification. *Ecol. Appl.* **2017**, *27*, 1677–1693. [CrossRef]
32. Dutrieux, L.; DeVries, B.; Verbesselt, J. BfastSpatial: Utilities to Monitor for Change on Satellite Image Time-Series. 2016. Available online: https://github.com/loicdtx/bfastSpatial (accessed on 28 December 2023).
33. Earthdata Search. *Earth Science Data and Information System (ESDIS) Project, Earth Science Projects Division (ESPD)*; NASA: Washington, DC, USA, 2019. Available online: https://www.earthdata.nasa.gov/ (accessed on 5 March 2023).
34. Hulley, G.; Hughes, C.G.; Hook, S.J. Quantifying Uncertainties in Land Surface Temperature and Emissivity Retrievals from ASTER and MODIS Thermal Infrared Data. *J. Geophys. Res. Atmos.* **2012**, *117*, D23113. [CrossRef]
35. Rouse, J.W.; Haas, R.H.; Schell, J.A.; Deering, D.W.; Harlan, J.C. *Monitoring the Vernal Advancement and Retrogradiation (Greenwave Effect) of Natural Vegetation*; NASA's Goddard Space Flight Center: Greenbelt, MD, USA, 1974.
36. Huang, S.; Tang, L.; Hupy, J.P.; Wang, Y.; Shao, G. A Commentary Review on the Use of Normalized Difference Vegetation Index (NDVI) in the Era of Popular Remote Sensing. *J. For. Res.* **2021**, *32*, 1–6. [CrossRef]
37. Ravibabu Mandla, V.; Vani, V. Comparative Study of NDVI and SAVI Vegetation Indices in Anantapur District Semi-Arid Areas. *Int. J. Civ. Eng. Technol.* **2017**, *8*, 559–566.
38. Hu, T.; Hulley, G.C.; Mallick, K.; Szantoi, Z.; Hook, S. Comparison between the ASTER and ECOSTRESS Global Emissivity Datasets. *Int. J. Appl. Earth Obs. Geoinf.* **2023**, *118*, 103227. [CrossRef]
39. Dybbroe, A.; Scheirer, R.; Raspaud, M.; Hoese, D.; Zhang, X.; Proud, S.R. Satellite Sensor Relative Spectral Response Data, Version v1.1.0 2022. Available online: https://zenodo.org/records/6557386 (accessed on 29 July 2022).
40. Brunsell, N.A.; Glllies, R.R. Incorporating Surface Emissivity into a Thermal Atmospheric Correction. *Photogramm. Eng. Remote Sens.* **2002**, *68*, 1263–1270.
41. Valor, E.; Caselles, V. Mapping Land Surface Emissivity from NDVI: Application to European, African, and South American Areas. *Remote Sens. Environ.* **1995**, *57*, 167–184. [CrossRef]
42. Garcia-Santos, V. Determination of the Surface Temperature by Remote Sensing. *Tethys J. Weather Clim. West. Mediterr.* **2010**, *7*, 67–74. [CrossRef]
43. Shen, Q.; Gao, G.; Han, F.; Xiao, F.; Ma, Y.; Wang, S.; Fu, B. Quantifying the Effects of Human Activities and Climate Variability on Vegetation Cover Change in a Hyper-Arid Endorheic Basin. *Land. Degrad. Dev.* **2018**, *29*, 3294–3304. [CrossRef]
44. Schmidt, H.; Karnieli, A. Sensitivity of Vegetation Indices to Substrate Brightness in Hyper-Arid Environment: The Makhtesh Ramon Crater (Israel) Case Study. *Int. J. Remote Sens.* **2001**, *22*, 3503–3520. [CrossRef]
45. Sobrino, J.A.; Jiménez-Muñoz, J.C.; Sòria, G.; Romaguera, M.; Guanter, L.; Moreno, J.; Plaza, A.; Martínez, P. Land Surface Emissivity Retrieval from Different VNIR and TIR Sensors. *IEEE Trans. Geosci. Remote Sens.* **2008**, *46*, 316–327. [CrossRef]
46. Schmidt, H.; Karnieli, A. Remote Sensing of the Seasonal Variability of Vegetation in a Semi-Arid Environment. *J. Arid. Environ.* **2000**, *45*, 43–59. [CrossRef]

47. Watts, L.M.; Laffan, S.W. Effectiveness of the BFAST Algorithm for Detecting Vegetation Response Patterns in a Semi-Arid Region. *Remote Sens. Environ.* **2014**, *154*, 234–245. [CrossRef]
48. Hulley, G.; Malakar, N.; Freepartner, R. *Moderate Resolution Imaging Spectroradiometer (MODIS) Land Surface Temperature and Emissivity Product (MxD21) Algorithm Theoretical Basis Document Collection 6.1*; JPL Publication: Pasadena, CA, USA, 2016.
49. García-Santos, V.; Coll, C.; Valor, E.; Niclòs, R.; Caselles, V. Analyzing the Anisotropy of Thermal Infrared Emissivity over Arid Regions Using a New MODIS Land Surface Temperature and Emissivity Product (MOD21). *Remote Sens. Environ.* **2015**, *169*, 212–221. [CrossRef]
50. Mira, M.; Valor, E.; Caselles, V.; Rubio, E.; Coll, C.; Galve, J.M.; Niclòs, R.; Sánchez, J.M.; Boluda, R. Soil Moisture Effect on Thermal Infrared (813-Mm) Emissivity. *IEEE Trans. Geosci. Remote Sens.* **2010**, *48*, 2251–2260. [CrossRef]
51. Krug, J. *Site-Species Matching and Planting Techniques for Arid-Zone Forestry in Namibia*; Cuvillier Verlag: Göttingen Germany, 2017.
52. Mu, X.; Hu, M.; Song, W.; Ruan, G.; Ge, Y.; Wang, J.; Huang, S.; Yan, G. Evaluation of Sampling Methods for Validation of Remotely Sensed Fractional Vegetation Cover. *Remote Sens.* **2015**, *7*, 16164–16182. [CrossRef]
53. Laliberte, A.S.; Rango, A.; Herrick, J.E.; Fredrickson, E.L.; Burkett, L. An Object-Based Image Analysis Approach for Determining Fractional Cover of Senescent and Green Vegetation with Digital Plot Photography. *J. Arid. Environ.* **2007**, *69*, 1–14. [CrossRef]